Research Article | Vol. 28, No. 21 / 12 October 2020 / Optics Express 31624
Optics EXPRESS

Silicon carbide as a material-based high-impedance surface for enhanced absorption within ultra-thin metallic films

JOSÉ M. PÉREZ-ESCUDERO,[1] IBAN BULDAIN,[1] MIGUEL BERUETE,[1,2] JAVIER GOICOECHEA,[1,2] AND IÑIGO LIBERAL[1,2,*]

[1]Department of Electrical and Electronic Engineering, Public University of Navarra, 31006 Pamplona, Spain
[2]Institute of Smart Cities, Public University of Navarra, 31006 Pamplona, Spain
[*]inigo.liberal@unavarra.es

Abstract: The absorption of infrared radiation within ultra-thin metallic films is technologically relevant for different thermal engineering applications and optoelectronic devices, as well as for fundamental research on sub-nanometer and atomically-thin materials. However, the maximal attainable absorption within an ultra-thin metallic film is intrinsically limited by both its geometry and material properties. Here, we demonstrate that material-based high-impedance surfaces enhance the absorptivity of the films, potentially leading to perfect absorption for optimal resistive layers, and a fourfold enhancement for films at deep nanometer scales. Moreover, material-based high-impedance surfaces do not suffer from spatial dispersion and the geometrical restrictions of their metamaterial counterparts. We provide a proof-of-concept experimental demonstration by using titanium nanofilms on top of a silicon carbide substrate.

1. Introduction

The absorption of infrared radiation by ultra-thin metallic films is the basic operating principle of a variety of systems including lightweight and dynamical thermal emitters [1–7], radiative cooling [8,9], thermal camouflage [10–13], thermal self-regulation or thermal homeostasis [14,15], sensors [16–18] and optoelectronic devices [19], to name a few. However, as we will discuss in detail, the maximal absorption that can be obtained in the limit of an ultra-thin metallic film is limited due to both (i) its ultra-thin film geometry, and (ii) the material properties of metals.

Perfect electromagnetic absorbers with a near 100% efficiency can be designed in a number of ways, including interference effects and internal resonances in thicker films [20,21], structuring the geometry of the film in the form of metasurfaces and metamaterials [22–28], multilayer systems [2,4,29], etc. However, concentrating the absorption within an unpatterned, ultra-thin, and metallic layer has several technological advantages. First, the fabrication of an ultra-thin metallic coating can be very simple, of particular interest for large-area and conformal applications. Second, metallic coatings quickly become opaque at optical frequencies as their thickness increases, and only ultra-thin films can be used in applications like smart windows and transparent electronics. For some applications like optoelectronic devices [19,30], only the power absorbed in the metallic film is of interest. Moreover, reducing the amount of material where the absorption takes place can both extend and speed up the reconfigurability of dynamical thermal emitters [5] and improve photothermal modulation [31]. Finally, maximizing the absorption in films entering sub-nanometer scales is relevant for fundamental research on nonlocal and quantum phenomena [32–35], and light-matter interactions within atomically-thin structures [36,37].

In this work, we propose the use of silicon carbide (SiC) as material-based high-impedance surface that enhances the absorption in ultra-thin metallic films while maintaining the aforementioned

#402397 https://doi.org/10.1364/OE.402397
Journal © 2020 Received 10 Jul 2020; revised 9 Sep 2020; accepted 9 Sep 2020; published 6 Oct 2020

Optics EXPRESS

technological advantages. Silicon carbide (SiC) [38,39] is a polar dielectric exhibiting a highly reflective band within the infrared atmospheric window, the Reststrahlen band, delimited by the transverse (TO) and longitudinal optic (LO) phonon frequencies. Within this band, SiC supports surface phonon polaritons (SPhPs) with lifetimes 3 orders of magnitude longer than those of plasmons in noble metals. With these exceptional optical properties, SiC enables the observation of extraordinary tranmission [40], superlensing [41], deeply subwavelength resonators [42,43], coherent thermal sources [44], sensing of sub-nanometric thin-films [35] and strong coupling with vibrational modes [45]. In addition, SiC exhibits a near-zero permittivity $\varepsilon\left(\lambda_p\right) \simeq 0$ around its plasma frequency $\lambda_p = 10.3\ \mu$m , being one of the highest-quality epsilon-near-zero (ENZ) materials known to date [46–48].

As the permittivity of a medium approaches zero, $\varepsilon \to 0$, its intrinsic impedance diverges $Z = Z_0/\sqrt{\varepsilon} \to \infty$, leading to a high-impedance boundary condition, similar to perfect magnetic conductor (PMC) boundary for sufficiently large bodies. In this manner, the tangential electric field is enhanced at the surface of a SiC substrate, while the tangential magnetic field is inhibited, leading to different light-matter interactions than those observed in dielectric and metallic substrates. In fact, high-impedance boundaries implemented with metamaterial structures have been extensively studied for suppressing surface waves [49], enhancing the efficiency of low-profile antennas [50–52], designing electromagnetic absorbers [53,54], and radar cross-section (RCS) reduction systems [55,56]. By contrast with metamaterial structures, SiC provides an intrinsic high-impedance boundary that does not suffer from spatial dispersion, does not require from nanofabrication, and preserves its behavior even in complex geometries with subwavelength details.

In the remainder of the manuscript we investigate how the intrinsic high-impedance boundary condition of SiC can be employed to enhance the absorption performance of ultra-thin metallic films. We note that while previous works have also focused on how absorption can be optimized inside ENZ bodies [57–59] or heterogeneous bodies composed of ENZ and dielectric and metal structures [20,60], our study focuses on how an intrinsic ENZ substrate boosts the absorption taking place within an ultra-thin metallic film.

2. Theory of absorption in ultra-thin metallic films

2.1. Equivalent circuit model

We start our discussion by considering the absorption properties and inherent limitations of ultra-thin metallic films by using an equivalent circuit model. To this end, we consider the geometry schematically depicted in Fig. 1(a), consisting of an ultra-thin metallic film, characterized by relative permittivity $\varepsilon_{\text{film}}(\omega)$ and thickness t, deposited on top of a substrate characterized by relative permittivity $\varepsilon_{\text{sub}}(\omega)$. We are interested in analysing the film in the *ultra-thin limit*, which we define as the case in which the film thickness is much smaller than the propagation length within the film. In this limit, there are no internal resonances in the slab, and its response can be described as an average electric current flowing through it [61]. Therefore, the response of the system can be accurately modelled by the equivalent circuit model shown in Fig. 1(b), and the contribution of the metallic film is given by the shunt impedance [61]

$$Z_{\text{film}}(\omega) = R_{\text{film}}(\omega) + j\,X_{\text{film}}(\omega) = \frac{1}{j\omega\varepsilon_0\chi(\omega)t} \tag{1}$$

where $\chi\left(\omega\right) = \varepsilon_{\text{film}}\left(\omega\right) - 1$ is the polarizability of the material composing the film. Since we consider a substrate of infinite extent, the substrate impedance is simply given by the intrinsic impedance of the substrate $Z_{\text{sub}}(\omega) = Z_0/\sqrt{\varepsilon_{\text{sub}}(\omega)}$. The electrical engineering $e^{j\omega t}$ time-convention is assumed and omitted hereafter.

One of the advantages of this circuit model is that it expedites the calculation of the power absorbed within the film, as it is directly represented by the power dissipated in the film resistance.

Optics EXPRESS

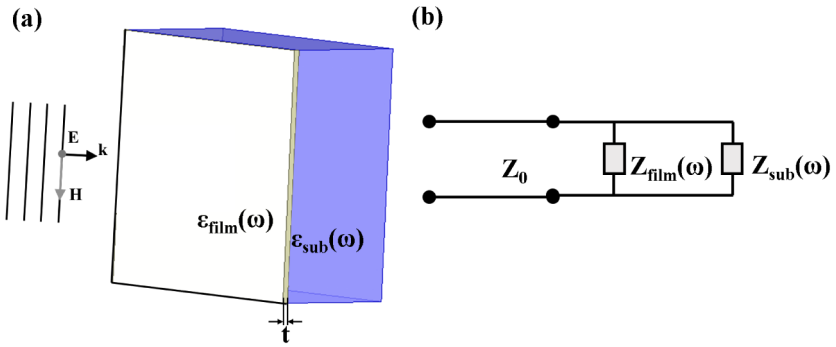

Fig. 1. (a) Sketch of the geometry: an ultra-thin metallic film characterized by relative permittivity $\varepsilon_{\text{film}}(\omega)$ and thickness t is deposited on top of a substrate characterized by relative permittivity $\varepsilon_{\text{sub}}(\omega)$. (b) Equivalent circuit model.

Therefore, the film absorptivity, i.e., the power absorbed by the thin film normalized to the incident power, can be written in circuital terms as follows

$$A_{\text{film}}(\omega) = 4\, Z_0\, R_{\text{film}}\, |\frac{Z_{\text{in}}}{Z_{\text{film}}(Z_{\text{in}} + Z_0)}|^2. \tag{2}$$

where $Z_{\text{in}}(\omega) = Z_{\text{film}} Z_{\text{sub}}/(Z_{\text{sub}} + Z_{\text{film}})$ is the input impedance.

2.2. Ultra-thin metallic films standing in air

The simple Eq. (2) allows to extract very useful information on the absorption properties of ultra-thin films. For example, for a film standing in air ($Z_{\text{sub}} = Z_0$) we can take derivatives with respect to the slab impedance to find that the absorption in the film is maximized for a purely resistive film $Z_{\text{film}} = Z_0/2$, leading to the following upper bound for the absorption coefficient $A_{\text{film}}(\omega) \leq 1/2$. This recovers the well-known result that a thin material layer can only absorb up to a half of the incident power.

Metallic layers are usually thought as thin resistive layers in the design of absorbers. However, this is only an approximation that does not hold for most metals at infrared frequencies. To illustrate this point, we study the absorption properties of a metallic film whose response can be approximated by that of a Drude dispersion model: $\varepsilon(\omega) = 1 - \omega_p^2/(\omega^2 - j\omega\omega_c)$, where ω_p and ω_c are the plasma and collision frequencies, respectively. Consequently, the film impedance is given by

$$Z_{\text{film}}(\omega) = j\omega(\frac{1}{\epsilon_0\omega_p^2 t}) + \omega_c(\frac{1}{\epsilon_0\omega_p^2 t}) = (j\omega + \omega_c)L \tag{3}$$

It is clear from Eq. (3) that thin metallic films are characterized by an intrinsic inductance, $L = (\epsilon_0\omega_p^2 t)^{-1}$, and a resistance that can be directly connected to the inductance through the collision frequency, i.e., $R = \omega_c L$. The fact that R and L are directly linked by the material properties imposes some restrictions on the absorptivity that can be obtained with a thin metallic film. Specifically, inserting this impedance into (2), we find that the absorption is maximized for the inductance value, $L = Z_0/2/\sqrt{\omega_c^2 - \omega^2}$, leading to the following upper bound for the absorptivity

$$A_{\text{film}}(\omega) \leq \frac{1}{1 + \sqrt{1 + \frac{\omega^2}{\omega_c^2}}} \tag{4}$$

In the $\omega_c \gg \omega$ limit the metallic film can be considered a purely resistive layer and we recover $A_{\text{film}}(\omega) \leq 1/2$. However, this condition does not hold for most metals at infrared frequencies.

Optics EXPRESS

Therefore, the material properties of metallic films, represented by their intrinsic inductance, further limits their absorptivity. This result poses the interesting perspective that, by contrast with most plasmonic systems [62], the absorption in ultra-thin metallic films can be larger for "lower-quality" materials with a higher collision frequency. As we will see, this conclusion is of practical importance for nanometric films, where detrimental effects such as surface roughness and impurities can effectively increase the collision frequency. This conclusion also constrasts with theoretical bounds on different nanophotonic processes, including absorption and thermal emission, where material losses are seen as a limiting factor [63,64]. The reason for this apparent disagreement is that such bounds assume the possibility of engineering the geometry of the material, while here we are interested in the case of a constrained geometry that is technologically advantageous.

A Drude model description is a good approximation for metals within some frequency windows, and it provides physical insight on the dominant dispersion effects. However, realistic metals present a more complex dispersion profile, including the contributions from interband transitions [65,66]. For an arbitrary material dispersion, maximizing the film thickness leads to an optimal value of $t = \omega^{-1} c \left|2\chi^{-1}\right|$ and the following upper-bound on absorption:

$$A_{\text{film}}(\omega) \leq \frac{1}{1 + \frac{\left|\chi^{-1}(\omega)\right|}{\text{Im}\left[\chi^{-1}(\omega)\right]}} \tag{5}$$

As an example of interest, we study the absorption characteristics of titanium (Ti) metal films, although other materials like chromium (Cr), platinum (Pt) or phase change materials in the metallic phase could be analyzed leading to similar conclusions. Figure 2 shows the absorptivity of Ti films of different thicknesses, as compared to the upper bound (4). As expected, the absorptivity always lies below its upper bound, but approaches it for certain combinations of thicknesses and wavelengths. These results also illustrate that Ti films at infrared frequencies do not behave exactly as resistive layers, presenting a nonnegligible material dispersion, and optimal absorption below the 1/2 thin film limit. Optimal absorption takes place for deeply subwavelength thicknesses, for example, for a wavelength of 10 μm the absorptivity is maximized for thicknesses between 6 nm and 8 nm ($0.0006\lambda \sim 0.0008\lambda$), for which there is an excellent agreement between the predictions of the circuit model and a full-wave numerical solver.

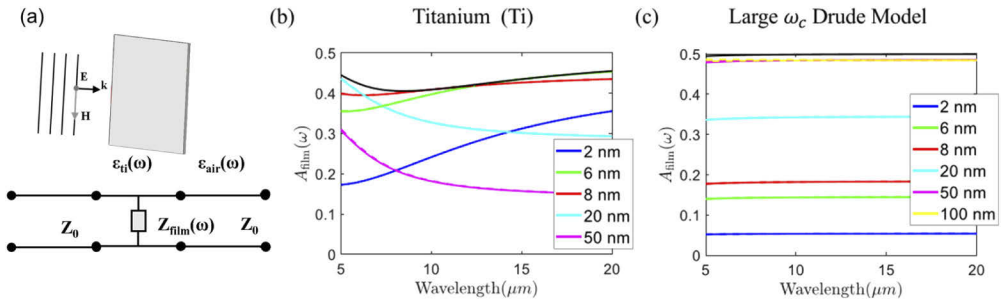

Fig. 2. (a) Sketch of a metallic film standing in air, and equivalent circuit model. (b) Predicted absorptivity spectrum for Ti films of different thicknesses, and comparison with the theoretical upper bound (solid black line). (c) Predicted absorptivity for a metallic thin film of different thicknesses, modeled with a Drude model with $\omega_p = 3.93 \times 10^{15}$rad/s and $\omega_c = 1.81 \times 10^{15}$rad/s. Solid lines correspond to a numerical simulation with a full-wave numerical solver, and dashed dot lines represent the prediction of the equivalent circuit model.

As anticipated, lower quality metals give access to larger absorptivities at infrared frequencies. In order to illustrate this point, Fig. 2(c) depicts the absorptivity for a metallic film characterized

Optics EXPRESS

by a Drude permittivity with parameters $\omega_p = 3.93 \times 10^{15}$rad/s and $\omega_c = 1.81 \times 10^{15}$rad/s, which is significantly lossier than the Drude component of Ti. In this case, the film behaves closer to a purely resistive layer, with an almost constant absorptivity spectrum that approaches the 1/2 limit for films with an optimal thickness. Specifically, the absorptivity is maximized for larger thicknesses between 50 nm and 100 nm. However, these are still deeply subwavelength thicknesses, for which the predictions of the circuit model perfectly match those of the full-wave numerical simulation.

2.3. Impact of the substrate on ultra-thin film absorption

The previous section clearly shows that the absorption in ultra-thin metallic films is limited by both its ultra-thin geometry and its material properties. Next, we explore how this limitation can be lifted by using material substrates. As shown in Fig. 3(a), we now assume that the thin-film is deposited on top of a substrate characterized by relative permittivity ε_{sub} , and characteristic impedance $Z_{\text{sub}} = n_{\text{sub}}^{-1} Z_0$ with $n_{\text{sub}} = \sqrt{\varepsilon_{\text{sub}}}$. Maximizing the absorption with respect to the film thickness leads to an optimal value of $t = \omega^{-1} c \left|(1 + n_{\text{sub}})\, \chi^{-1}\right|$, and the following upper bound for the film's absorptivity

$$A_{\text{film}}(\omega) \leq 2\, \frac{\text{Im}\left[\chi^{-1}\right]}{\left|(1 + n_{\text{sub}})\, \chi^{-1}\right| + \text{Im}\left[(1 + n_{\text{sub}})\, \chi^{-1}\right]} \tag{6}$$

In the limit of a resistive layer ($\text{Re}\left[\chi^{-1}\right] \to 0$) on top of a zero-index substrate ($n_{\text{sub}} \to 0$, $Z_{\text{sub}} \to \infty$) the upper bound converges to unity, indicating the possibility of designing a perfect absorber. In such a limit, the system behaves similar to conventional high-impedance surface absorbers [53,54], with the only difference that the high-impedance surface is provided by the material properties of the substrate. In general, Eq. (6) represents a tighter bound, providing an estimation of the absorption that can be obtained with realistic materials in an ultra-thin film / substrate configuration. In fact, Eq. (6) only contains material parameters.

A particularly relevant case is that of substrates with a purely real refractive index, for which the contribution of n_{sub} in Eq. (6) simplifies to a multiplicative factor $(1 + n_{\text{sub}})^{-1}$. It is then clear that dielectric substrates with $n_{\text{sub}}>1$ can only limit the absorption of ultra-thin metallic films deposited on top of them, while substrates with a near-zero refractive index $n_{\text{sub}} \simeq 0$ enhance the absorption of any thin-film material.

However, near-zero-index substrates at infrared frequencies are typically based on lossy ENZ media for which $\varepsilon_{\text{sub}}(\omega_{\text{ENZ}}) = -j\delta$. The real and imaginary parts of the associated refractive index are equally important, $n_{\text{sub}}(\omega_{\text{ENZ}}) = \sqrt{\delta/2}\,(1 - j)$, leading to a complex interplay between substrate and film. From a circuital standpoint, this interplay arises from the fact that the reactance of the substrate can help to compensate the intrinsic inductance of a metallic layer.

As a particular example, we investigate the use of silicon carbide (SiC) as a near-zero-index substrate. SiC can be modelled with a Lorentzian dispersion profile $\varepsilon_{\text{SiC}} = (\omega^2 - \omega_p^2 - j\omega\omega_c)/(\omega^2 - \omega_0^2 - j\omega\omega_c)$, with $\omega_p = 2\pi c/(10.3 \times 10^{-6})$ rad/s, $\omega_0 = 2\pi c/(12.55 \times 10^{-6})$ rad/s, and $\omega_c = 0.0022\omega_0$, so that the real part of the relative permittivity crosses zero at thermal infrared frequencies [38,67] (see Fig. 3(b)). The absorptivities of the Ti films studied in Fig. 2(b), but deposited on top of a SiC substrate are reported in Fig. 3(c). It is clear from the figure that the absorption spectrum now closely follows the material dispersion of the substrate, with an enhanced peak absorptivity within the film near 0.7. In this case, the maximal absorption is obtained for thinner films around 6 nm, then the absorptivity decreases as the thickness increases, consistent with the fact that the optimal thickness, $t = \omega^{-1} c \left|(1 + n_{\text{sub}})\chi^{-1}\right|$, monotonically increases along with the substrate refractive index.

Similar to thin films standing in air, higher absorptivities are obtained for metal layers with a response closer to that of purely resistive layers. Figure 3(d) depicts the absorptivities predicted

Optics EXPRESS

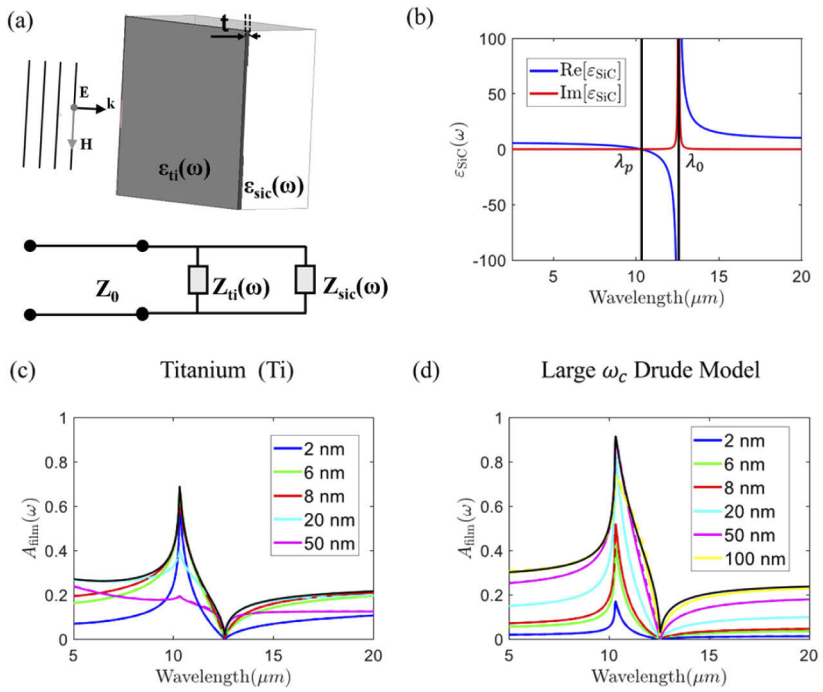

Fig. 3. (a) Sketch of a metallic film on top of an silicon carbide (SiC) substrate, and equivalent circuit model. (b) Real (blue) and Imaginary (red) permittivity of Silicon Carbide (SiC). Black lines correspond to plasma (λ_p) and resonance (λ_0) frequencies. (c) Predicted absorptivity spectrum for Ti films of different thicknesses on top of a SiC substrate, and comparison with the theoretical upper bound (solid black line). (d) Predicted absorptivity for a metallic thin film of different thicknesses, modeled with a Drude model with $\omega_p = 3.93 \times 10^{15}$rad/s and $\omega_c = 1.81 \times 10^{15}$rad/s. Solid lines correspond to a numerical simulation with a full-wave numerical solver, and dashed dot lines represent the prediction of the equivalent circuit model.

for a Drude model dispersion with a high collision frequency. Again, the absorptivity spectra is characterized by a maximum-minimum sequence following the material dispersion of the substrate. The absorptivity is increased as the thickness increases until the maximal absorption of 0.91 is achieved for metal films around 50 nm thickness. Then, the absorptivity decreases as the thickness is increased.

2.4. Sub-nanometer and atomically-thin films

Of particular scientific interest is also the limit of metallic films entering sub-nanometer and atomically-thin scales [35–37]. In such limit, the response of a film cannot be accurately described with the same material parameters than those of the bulk material. However, size-dependent corrected material parameters can still be employed [68,69], for which our theory can be applied.

At the same time, the application of this theory to sub-nanometer and atomically-thin films presents its own particularities. Specifically, the film impedance (1) becomes much larger than the substrate impedance $Z_{\text{film}} \gg Z_{\text{sub}}$, so that we can approximate the input impedance by $Z_{\text{in}} \simeq Z_{\text{sub}}$, and the absorptivity reduces to

$$A_{\text{film}}(\omega) = 4\,Z_0\,\frac{R_{\text{film}}}{|Z_{\text{film}}|^2}\left|\frac{Z_{\text{sub}}}{Z_{\text{sub}}+Z_0}\right|^2. \tag{7}$$

Optics EXPRESS

It is clear from Eq. (7) that in this limit the impact of the substrate reduces to a multiplicative factor. This motivates the definition of an absorptivity enhancement factor, given by the ratio of absorptivities with and without the substrate, which can be written as follows

$$\mathrm{EF}(\omega) = 4\,\frac{1}{|1+n_{\mathrm{sub}}|^2} \tag{8}$$

This limit can be understood as a consequence from the fact that sub-nanometric and atomically-thin films have a negligible impact on the local field, and the enhancement factor is directly given by the enhancement of the electric field intensity induced by the substrate in the absence of the film. Therefore, although sub-nanometer and atomically-thin metallic layers have a very low absorption efficiency, their absorptivity can be increased by a factor of 4 by using an ideal near-zero-index substrate. Near-zero permittivities of $\varepsilon_{\mathrm{sub}} = -j\,0.01$, $\varepsilon_{\mathrm{sub}} = -j\,0.1$, $\varepsilon_{\mathrm{sub}} = -j\,0.2$ and $\varepsilon_{\mathrm{sub}} = -j\,0.5$, would lead to enhancements factors of 3.47, 2.59, 2.18 and 1.6, suggesting that this effect could be observed in a large number of practical ENZ materials [46–48]. To illustrate this conclusion, Fig. 4 represents the absorptivity enhancement factor for Ti films with and without a SiC substrate, as a function of the film thickness. As anticipated, the enhancement factor is maximized at the plasma frequency of SiC, and its peak value decreases as the slab thickness increases. To finalize, we note that the $Z_{\mathrm{film}} >> Z_{\mathrm{sub}}$ limit might appear to be in conflict with the use of ENZ substrates with a diverging impedance. However, the film impedance of sub-nanometric and atomically-thin films quickly overcomes that of realistic ENZ materials, thus justifying the use of the limit. Moreover, even if an ideal ENZ material with an infinite characteristic impedance would be considered, the result of the limit would be the same. According to the circuit model depicted in Fig. 3(a), both the film impedance and the substrate impedance would become open circuits, leading to the aforementioned fourfold enhancement on the absorptivity.

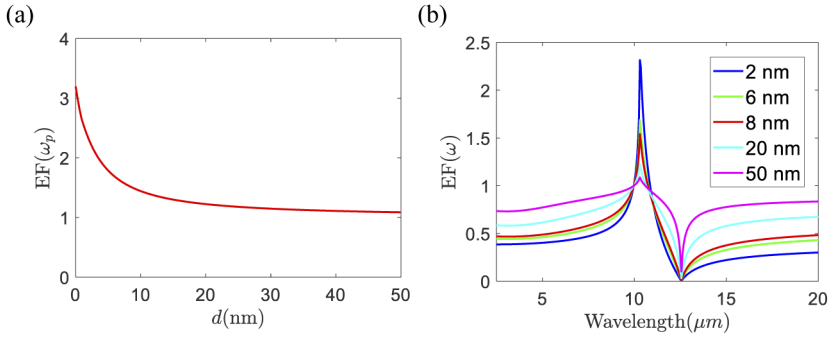

Fig. 4. (a) Absorptivity enhancement factor *EF* at the plasma frequency of silicon carbide (SiC) for a titanium (Ti) film with and without a SiC substrate, as a function of the Ti film thickness. (b) Spectra of the absorptivity enhancement factor for different Ti film thicknesses.

2.5. *Geometrical flexibility of material-based high-impedance surfaces*

An important advantage of material-based high-impedance surfaces is that they do not suffer from spatial dispersion and the geometrical restrictions of their metamaterial counterparts. For example, the radius of curvature of the surface is not restricted by the size of a unit-cell, and the field distribution is preserved even at deeply subwavelength scales. In order to illustrate this effect, we numerically investigate the absorptivity of a Ti film deposited on top of a SiC substrate with an irregular profile described by the periodic function $x(y) = A_1 \sin(k_1 y) + A_2 \sin(k_2 y) + A_3 \sin(k_3 y)$, with $A_1 = L/40$, $A_2 = L/10$ and $A_3 = L/30$, and $k_1 = 2\pi\,2/L$, $k_2 = 2\pi\,4/L$ and $k_3 = 2\pi\,4/L$

Optics EXPRESS

(see Fig. 5(a)). Here, L is defined as a length parameter that describes the overall scale of the system. Figure 5(b) reports the absorptivity of the Ti film for three length scales: subwavelength $L = 500$ nm, comparable to the wavelength $L = 5$ μm and larger than the wavelength, $L = 50$ μm. It can be concluded that the absorptivity of the film presents the expected maxima/minima profile for all length scales. As the length scale increases, a ripple appears on the absorptivity due to the presence of interference phenomena in the irregular substrate. However, the general trend in the absorptivity spectrum is dominated by the dispersion of the substrate. Therefore, these results confirm that material-based impedance substrate can operate even in irregular substrates of different length scales.

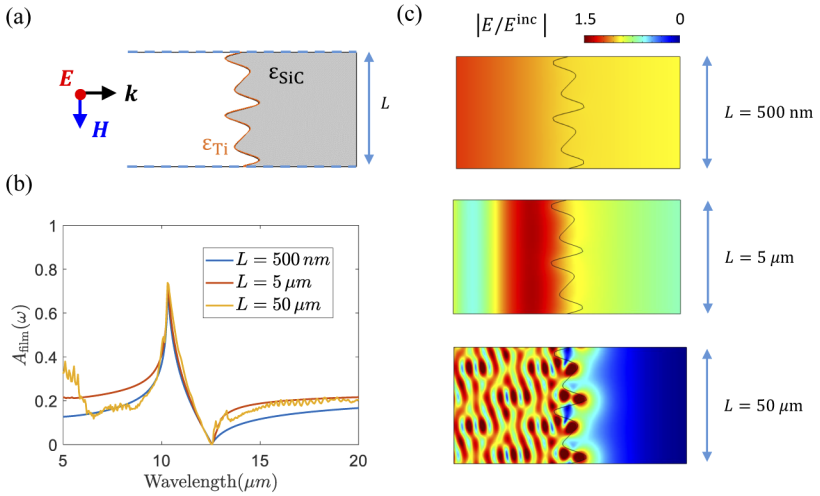

Fig. 5. (a) Sketch of a titanium (Ti) film of 2 nm thickness deposited on top of a silicon carbide (SiC) substrate with an irregular profile described by the periodic function $x(y) = A_1 \sin(k_1 y) + A_2 \sin(k_2 y) + A_3 \sin(k_3 y)$, with $A_1 = L/40$, $A_2 = L/10$ and $A_3 = L/30$, and $k_1 = 2\pi\, 2/L$, $k_2 = 2\pi\, 4/L$ and $k_3 = 2\pi\, 4/L$, where L is a length parameter that describes the overall scale of the system. (b) Absorptivity if the Ti film for length scales $L = 500$ nm, $L = 5$ μm and , $L = 50$ μm. (c) Electric field magnitude at the plasma frequency of the SiC substrate for the different length scales.

In order to provide additional physical insight on this effect, Fig. 5(c) reports the electric field distributions at the plasma frequency of the SiC substrate. Different regimes are observed at each length scale, and the field distribution evolves from a near constant distribution at subwavelength scales, to a complex distribution arising from interference phenomena at scales larger than the wavelength. At the same time, the electric field is maximized near the surface for all length scales, thus enhancing the film absortivity.

3. Experimental results

We provide a proof-of-concept experimental demonstration by depositing Ti films of 2, 6, 8, 20 and 50 nm thickness on top of a SiC substrate. The fabrication of the samples is photolithograpy-free and has been realized evaporating Ti on a 220 μm thick SiC substrate. No passive layer was used to prevent oxidation, since Ti reacts with the air leading to an spontaneous passivation layer, consisting of around 1 nm of amorphous TiO_2, which protects it against corrosion and further oxidation [70,71]. Figure 6(a) shows a picture of the fabricated samples where it can be appreciated the transition from transparent to opaque as the thickness increases. Figure 6(b) shows a SEM image of the 50 nm film, revealing that the evaporated thin films present a large roughness as it has been observed in related works [2,3]. The root mean square roughness (Rq)

Optics EXPRESS

is around 2 nm, exhibiting geometrical details comparable to the thickness of the films. The full characterization of the sample roughness via atomic force microscopy is reported in Supplement 1, Fig. S1. Therefore, the roughness is expected to have an important impact on the response of the film. Intuitively, it should be expected that the roughness increases the resistivity of the layer, and our experimental data fit to the Drude model with a high-collision frequency described in the theory section. Note that as it has been discussed, resistive layers actually provide higher absorptivities.

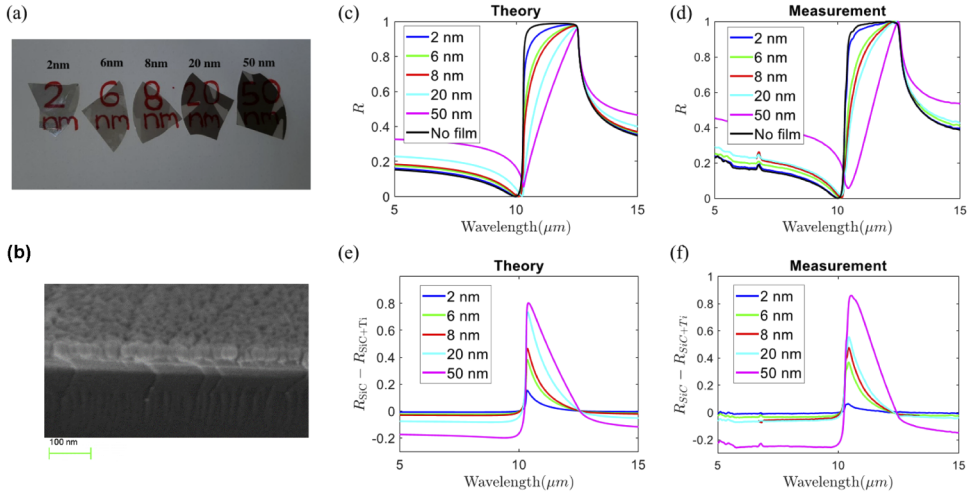

Fig. 6. (a) Photograph of the fabricated prototypes showing the transition from transparent to opaque samples. (b) SEM image of the 50 nm thin-film on SiC. (c) Prediction and (d) measurement of the reflectivity from Ti films of different thicknesses on top of SiC. (e) Prediction and (f) measurement of the reflectivity difference $R_{SiC} - R_{SiCTi}$.

We characterized the fabricated samples by means of reflectivity measurements via FTIR spectroscopy. The predicted and measured reflectivities are reported in Figs. 6(c) and 6(d), respectively, showing and excellent agreement between theory and measurements. The measured reflectivities are characterized by a highly reflective band between 10.3 μm and 12.55 μm, corresponding to SiC Reststrahlen band [38]. In addition, the reflectivity within this band decreases when a Ti film of increasing thickness is deposited on top of the SiC substrate.

Reflectivity measurements do not allow for a direct estimation of the power absorbed within the Ti thin film. However, a related figure of merit is the reflectivity difference for the substrate with and without the sample, $R_{\mathrm{SiC}} - R_{\mathrm{SiC+Ti}}$, whose predicted and measured values are reported in Figs. 6(e) and 6(f), respectively. This figure of merit provides an accurate description for the film absorptivity within the Reststrahlen band (see Supplement 1, Fig. S2 for a theoretical comparison of the reflectivity difference and the film absorptivity), and it is characterized by a peak and zero sequence, corresponding to the plasma and resonant frequencies of the SiC substrate. Therefore, the experimental results demonstrate that the absorptivity of the film follows the dispersion of the material substrate, and it is maximized around its plasma frequency. We note that the transmission through the substrate is near zero in all cases. However, outside the Reststrahlen band, the reflectivity difference becomes negative, with the physical implication than a metallic thin-film increases the reflection from a dielectric. Nonetheless, within the band of interest the reflectivity difference exhibits positive values matching those of the film absorptivity. This matching is justified by the fact that the absorption within the metallic thin-film forces the reflection to be lower than that of the bare substrate. The maximal value of this figure of merit

Optics EXPRESS

rises up to 0.88 for a 50 nm film thickness near the plasma frequency, evidencing a large film absorptivity.

Figure 7 depicts the magnitude of the reflectivity difference for different Ti film thicknesses normalized to its maximal value. This normalization highlights that the spectral features of the reflectivity become narrower as the film thickness decreases. This result is consistent with the narrowing of the absorptivity and the larger enhancement factors observed in the theoretical of increasingly thinner films.

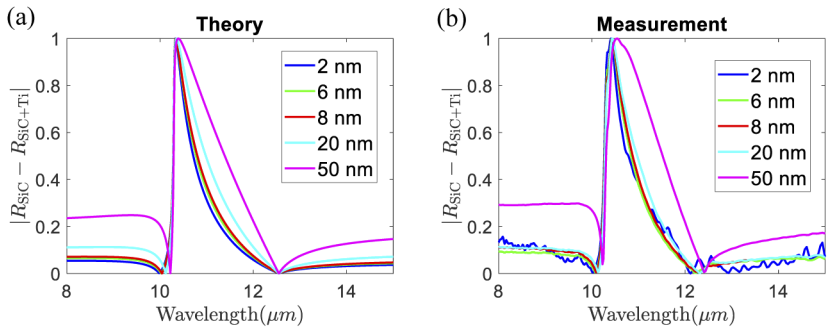

Fig. 7. (a) Prediction and (b) measurement of the magnitude of the reflectivity difference $|R_{SiC} - R_{SiC+Ti}|$, normalized to its maximum value for Ti films of different thicknesses deposited on top of a SiC substrate.

4. Conclusions

Our results provide a comprehensive view of how the absorptivity of ultra-thin metallic films is inherently limited by both their ultra-thin geometry and the material properties of metals. Furthermore, we theoretically and experimentally demonstrate that material-based high-impedance surfaces enhance the absorptivity, enabling perfect absorption for optimal resistive layers and up to a fourfold enhancement for sub-nanometer thin films. The possibility of enhancing the absorption of infrared radiation, while at the same time preserving technological advantages such as ease of fabrication, geometrical-flexibility and integrability, suggests that material-based high-impedance surfaces might find applications in thermal engineering and optoelectronic devices, as well as for fundamental research on light-matter interactions at sub-nanometric and atomically-thin scales.

Funding

Horizon 2020 Framework Programme (ATTRACT ENZSICSENS); Ministerio de Ciencia, Innovación y Universidades (RTI2018-093714- 301 J-I00, RYC2018-024123-I).

Acknowledgments

I.L. acknowledges support from ATTRACT project ENZSICSENS sponsored by H2020, Ramón y Cajal fellowship RYC2018-024123-I and project RTI2018-093714- 301 J-I00 sponsored by MCIU/AEI/FEDER/UE.

Disclosures

The authors declare no conflicts of interest.

Optics EXPRESS

See Supplement 1 for supporting content.

References

1. D. G. Baranov, Y. Xiao, I. A. Nechepurenko, A. Krasnok, A. Alù, and M. A. Kats, "Nanophotonic engineering of far-field thermal emitters," Nat. Mater. **18**(9), 920–930 (2019).
2. A. Naqavi, S. P. Loke, M. D. Kelzenberg, D. M. Callahan, T. Tiwald, E. C. Warmann, P. Espinet-González, N. Vaidya, T. A. Roy, J.-S. Huang, T. G. Vinogradova, and H. A. Atwater, "Extremely broadband ultralight thermally-emissive optical coatings," Opt. Express **26**(14), 18545–18562 (2018).
3. Z. Li, E. Palacios, S. Butun, H. Kocer, and K. Aydin, "Omnidirectional, broadband light absorption using large-area, ultrathin lossy metallic film coatings," Sci. Rep. **5**(1), 15137 (2015).
4. J. Park, J.-H. Kang, X. Liu, S. J. Maddox, K. Tang, P. C. McIntyre, S. R. Bank, and M. L. Brongersma, "Dynamic thermal emission control with inas-based plasmonic metasurfaces," Sci. Adv. **4**(12), eaat3163 (2018).
5. E. Sakat, L. Wojszvzyk, J.-P. Hugonin, M. Besbes, C. Sauvan, and J.-J. Greffet, "Enhancing thermal radiation with nanoantennas to create infrared sources with high modulation rates," Optica **5**(2), 175–179 (2018).
6. T. Inoue, M. De Zoysa, T. Asano, and S. Noda, "Realization of dynamic thermal emission control," Nat. Mater. **13**(10), 928–931 (2014).
7. L. Cai, K. Du, Y. Qu, H. Luo, M. Pan, M. Qiu, and Q. Li, "Nonvolatile tunable silicon-carbide-based midinfrared thermal emitter enabled by phase-changing materials," Opt. Lett. **43**(6), 1295–1298 (2018).
8. A. P. Raman, M. A. Anoma, L. Zhu, E. Rephaeli, and S. Fan, "Passive radiative cooling below ambient air temperature under direct sunlight," Nature **515**(7528), 540–544 (2014).
9. W. Li and S. Fan, "Nanophotonic control of thermal radiation for energy applications," Opt. Express **26**(12), 15995–16021 (2018).
10. M. A. Kats, R. Blanchard, S. Zhang, P. Genevet, C. Ko, S. Ramanathan, and F. Capasso, "Vanadium dioxide as a natural disordered metamaterial: perfect thermal emission and large broadband negative differential thermal emittance," Phys. Rev. X **3**(4), 041004 (2013).
11. Y. Qu, Q. Li, L. Cai, M. Pan, P. Ghosh, K. Du, and M. Qiu, "Thermal camouflage based on the phase-changing material gst," Light: Sci. Appl. **7**(1), 26 (2018).
12. Y. Qu, Q. Li, K. Du, L. Cai, J. Lu, and M. Qiu, "Dynamic thermal emission control based on ultrathin plasmonic metamaterials including phase-changing material gst," Laser Photonics Rev. **11**(5), 1700091 (2017).
13. A. Shahsafi, P. Roney, Y. Zhou, Z. Zhang, Y. Xiao, C. Wan, R. Wambold, J. Salman, Z. Yu, and J. Li, "Temperature-independent thermal radiation," Proc. Natl. Acad. Sci. **116**(52), 26402–26406 (2019).
14. S.-H. Wu, M. Chen, M. T. Barako, V. Jankovic, P. W. Hon, L. A. Sweatlock, and M. L. Povinelli, "Thermal homeostasis using microstructured phase-change materials," Optica **4**(11), 1390–1396 (2017).
15. M. Ono, K. Chen, W. Li, and S. Fan, "Self-adaptive radiative cooling based on phase change materials," Opt. Express **26**(18), A777–A787 (2018).
16. N. Liu, M. Mesch, T. Weiss, M. Hentschel, and H. Giessen, "Infrared perfect absorber and its application as plasmonic sensor," Nano Lett. **10**(7), 2342–2348 (2010).
17. G. Li, X. Chen, O. Li, C. Shao, Y. Jiang, L. Huang, B. Ni, W. Hu, and W. Lu, "A novel plasmonic resonance sensor based on an infrared perfect absorber," J. Phys. D: Appl. Phys. **45**(20), 205102 (2012).
18. F. Cheng, X. Yang, and J. Gao, "Enhancing intensity and refractive index sensing capability with infrared plasmonic perfect absorbers," Opt. Lett. **39**(11), 3185–3188 (2014).
19. L. J. Krayer, J. Kim, J. L. Garreta, and J. N. Munday, "Optoelectronic devices on indez-near-zero substrates," ACS Photonics **6**(9), 2238–2244 (2019).
20. M. A. Kats, R. Blanchard, P. Genevet, and F. Capasso, "Nanometre optical coatings based on strong interference effects in highly absorbing media," Nat. Mater. **12**(1), 20–24 (2013).
21. J. Rensberg, Y. Zhou, S. Richter, C. Wan, S. Zhang, P. Schöppe, R. Schmidt-Grund, S. Ramanathan, F. Capasso, and M. A. Kats, "Epsilon-near-zero substrate engineering for ultrathin-film perfect absorbers," Phys. Rev. Appl. **8**(1), 014009 (2017).
22. N. I. Landy, S. Sajuyigbe, J. J. Mock, D. R. Smith, and W. J. Padilla, "Perfect metamaterial absorber," Phys. Rev. Lett. **100**(20), 207402 (2008).
23. C. M. Watts, X. Liu, and W. J. Padilla, "Metamaterial electromagnetic wave absorbers," Adv. Mater. **24**(23), OP98–OP120 (2012).
24. G. M. Akselrod, J. Huang, T. B. Hoang, P. T. Bowen, L. Su, D. R. Smith, and M. H. Mikkelsen, "Large-area metasurface perfect absorbers from visible to near-infrared," Adv. Mater. **27**(48), 8028–8034 (2015).
25. Q. Feng, M. Pu, C. Hu, and X. Luo, "Engineering the dispersion of metamaterial surface for broadband infrared absorption," Opt. Lett. **37**(11), 2133–2135 (2012).
26. Y. W. Y. Guo, Y. Wang, M. Pu, Z. Zhao, X. Wu, X. Ma, C. Wang, L. Yan, and X. Luo, "Dispersion management of anisotropic metamirror for super-octave bandwidth polarization conversion," Sci. Rep. **5**(1), 8434 (2015).
27. X. Wu, T. Fan, T. G. Allen, S. Abdollahramezani, A. A. Eftekhar, M. Bosi, J. W. Perry, and A. Adibi, "Nonvolatile tunable integrated mid-infrared gst-sic metasurfaces," in *2018 IEEE Photonics Conference (IPC)*, (2018), pp. 1–2.

Optics EXPRESS

28. Y. Yang, S. Taylor, H. Alshehri, and L. Wang, "Wavelength-selective and diffuse infrared thermal emission mediated by magnetic polaritons from silicon carbide metasurfaces," Appl. Phys. Lett. **111**(5), 051904 (2017).
29. P. Rodríguez-Ulibarri, M. Beruete, and A. E. Serebryannikov, "One-way quasiplanar terahertz absorbers using nonstructured polar dielectric layers," Phys. Rev. B **96**(15), 155148 (2017).
30. T. Yatsui, "Recent improvement of silicon absorption in opto-electric devices," Opto-Electron. Adv. **2**(10), 19002301–19002308 (2019).
31. E. J. Dias, R. Yu, and F. J. G. de Abajo, "Thermal manipulation of plasmons in atomically thin films," Light: Sci. Appl. **9**(1), 87 (2020).
32. D. De Ceglia, M. Scalora, M. A. Vincenti, S. Campione, K. Kelley, E. L. Runnerstrom, J.-P. Maria, G. A. Keeler, and T. S. Luk, "Viscoelastic optical nonlocality of low-loss epsilon-near-zero nanofilms," Sci. Rep. **8**(1), 9335 (2018).
33. N. A. Mortensen, S. Raza, M. Wubs, T. Søndergaard, and S. I. Bozhevolnyi, "A generalized non-local optical response theory for plasmonic nanostructures," Nat. Commun. **5**(1), 3809 (2014).
34. W. Zhu, R. Esteban, A. G. Borisov, J. J. Baumberg, P. Nordlander, H. J. Lezec, J. Aizpurua, and K. B. Crozier, "Quantum mechanical effects in plasmonic structures with subnanometre gaps," Nat. Commun. **7**(1), 11495 (2016).
35. R. Berte, C. R. Gubbin, V. D. Wheeler, A. J. Giles, V. Giannini, S. A. Maier, S. De Liberato, and J. D. Caldwell, "Sub-nanometer thin oxide film sensing with localized surface phonon polaritons," ACS Photonics **5**(7), 2807–2815 (2018).
36. Z. M. Abd El-Fattah, V. Mkhitaryan, J. Brede, L. Fernández, C. Li, Q. Guo, A. Ghosh, A. R. Echarri, D. Naveh, and F. Xia, "Plasmonics in atomically thin crystalline silver films," ACS Nano **13**(7), 7771–7779 (2019).
37. A. Manjavacas and F. J. García De Abajo, "Tunable plasmons in atomically thin gold nanodisks," Nat. Commun. **5**(1), 3548 (2014).
38. J. D. Caldwell, L. Lindsay, V. Giannini, I. Vurgaftman, T. L. Reinecke, S. A. Maier, and O. J. Glembocki, "Low-loss, infrared and terahertz nanophotonics using surface phonon polaritons," Nanophotonics **4**(1), 44–68 (2015).
39. W. Spitzer, D. Kleinman, and D. Walsh, "Infrared properties of hexagonal silicon carbide," Phys. Rev. **113**(1), 127–132 (1959).
40. Y. Urzhumov, D. Korobkin, B. Neuner III, C. Zorman, and G. Shvets, "Optical properties of sub-wavelength hole arrays in sic membranes," J. Opt. A: Pure Appl. Opt. **9**(9), S322–S333 (2007).
41. T. Taubner, D. Korobkin, Y. Urzhumov, G. Shvets, and R. Hillenbrand, "Near-field microscopy through a sic superlens," Science **313**(5793), 1595 (2006).
42. J. D. Caldwell, O. J. Glembocki, Y. Francescato, N. Sharac, V. Giannini, F. J. Bezares, J. P. Long, J. C. Owrutsky, I. Vurgaftman, and J. G. Tischler, "Low-loss, extreme subdiffraction photon confinement via silicon carbide localized surface phonon polariton resonators," Nano Lett. **13**(8), 3690–3697 (2013).
43. A. M. Dubrovkin, B. Qiang, T. Salim, D. Nam, N. I. Zheludev, and Q. J. Wang, "Resonant nanostructures for highly confined and ultra-sensitive surface phonon-polaritons," Nat. Commun. **11**(1), 1863 (2020).
44. J.-J. Greffet, R. Carminati, K. Joulain, J.-P. Mulet, S. Mainguy, and Y. Chen, "Coherent emission of light by thermal sources," Nature **416**(6876), 61–64 (2002).
45. T. G. Folland, G. Lu, A. Bruncz, J. R. Nolen, M. Tadjer, and J. D. Caldwell, "Vibrational coupling to epsilon-near-zero waveguide modes," ACS Photonics **7**(3), 614–621 (2020).
46. I. Liberal and N. Engheta, "Near-zero refractive index photonics," Nat. Photonics **11**(3), 149–158 (2017).
47. N. Kinsey, C. Devault, A. Boltasseva, and V. M. Shalaev, "Near-zero-index materials for photonics," Nat. Rev. Mater. pp. 1–19 (2019).
48. O. Reshef, I. De Leon, M. Z. Alam, and R. W. Boyd, "Nonlinear optical effects in epsilon-near-zero media," Nat. Rev. Mater. **4**(8), 535–551 (2019).
49. D. Sievenpiper, L. Zhang, R. F. Broas, N. G. Alexopolous, and E. Yablonovitch, "High-impedance electromagnetic surfaces with a forbidden frequency band," IEEE Trans. Microwave Theory Tech. **47**(11), 2059–2074 (1999).
50. A. P. Feresidis, G. Goussetis, S. Wang, and J. C. Vardaxoglou, "Artificial magnetic conductor surfaces and their application to low-profile high-gain planar antennas," IEEE Trans. Antennas Propag. **53**(1), 209–215 (2005).
51. D. F. Sievenpiper, J. H. Schaffner, H. J. Song, R. Y. Loo, and G. Tangonan, "Two-dimensional beam steering using an electrically tunable impedance surface," IEEE Trans. Antennas Propag. **51**(10), 2713–2722 (2003).
52. F. Costa, A. Monorchio, S. Talarico, and F. M. Valeri, "An active high-impedance surface for low-profile tunable and steerable antennas," Antennas Wirel. Propag. Lett. **7**, 676–680 (2008).
53. S. A. Tretyakov and S. I. Maslovski, "Thin absorbing structure for all incidence angles based on the use of a high-impedance surface," Microw. Opt. Technol. Lett. **38**(3), 175–178 (2003).
54. D. Kern and D. H. Werner, "A genetic algorithm approach to the design of ultra-thin electromagnetic bandgap absorbers," Microw. Opt. Technol. Lett. **38**(1), 61–64 (2003).
55. M. Paquay, J.-C. Iriarte, I. Ederra, R. Gonzalo, and P. de Maagt, "Thin amc structure for radar cross-section reduction," IEEE Trans. Antennas Propag. **55**(12), 3630–3638 (2007).
56. T. J. Cui, M. Q. Qi, X. Wan, J. Zhao, and Q. Cheng, "Coding metamaterials, digital metamaterials and programmable metamaterials," Light: Sci. Appl. **3**(10), e218 (2014).
57. S. Vassant, J.-P. Hugonin, F. Marquier, and J.-J. Greffet, "Berreman mode and epsilon near zero mode," Opt. Express **20**(21), 23971–23977 (2012).
58. S. Molesky, C. J. Dewalt, and Z. Jacob, "High temperature epsilon-near-zero and epsilon-near-pole metamaterial emitters for thermophotovoltaics," Opt. Express **21**(S1), A96–A110 (2013).

Optics EXPRESS

59. E. L. Runnerstrom, K. P. Kelley, E. Sachet, C. T. Shelton, and J.-P. Maria, "Epsilon-near-zero modes and surface plasmon resonance in fluorine-doped cadmium oxide thin films," ACS Photonics **4**(8), 1885–1892 (2017).
60. I. Liberal and N. Engheta, "Manipulating thermal emission with spatially static fluctuating fields in arbitrarily shaped epsilon-near-zero bodies," Proc. Natl. Acad. Sci. **115**(12), 2878–2883 (2018).
61. S. Tretyakov, *Analytical modeling in applied electromagnetics* (Artech House, 2003).
62. J. B. Khurgin, "How to deal with the loss in plasmonics and metamaterials," Nat. Nanotechnol. **10**(1), 2–6 (2015).
63. O. D. Miller, A. G. Polimeridis, M. H. Reid, C. W. Hsu, B. G. DeLacy, J. D. Joannopoulos, M. Soljačić, and S. G. Johnson, "Fundamental limits to optical response in absorptive systems," Opt. Express **24**(4), 3329–3364 (2016).
64. O. D. Miller, S. G. Johnson, and A. W. Rodriguez, "Shape-independent limits to near-field radiative heat transfer," Phys. Rev. Lett. **115**(20), 204302 (2015).
65. A. D. Rakić, A. B. Djurišić, J. M. Elazar, and M. L. Majewski, "Optical properties of metallic films for vertical-cavity optoelectronic devices," Appl. Opt. **37**(22), 5271–5283 (1998).
66. P. B. Johnson and R. W. Christy, "Optical constants of the noble metals," Phys. Rev. B **6**(12), 4370–4379 (1972).
67. J. Kim, A. Dutta, G. V. Naik, A. J. Giles, F. J. Bezares, C. T. Ellis, J. G. Tischler, A. M. Mahmoud, H. Caglayan, and O. J. Glembocki, "Role of epsilon-near-zero substrates in the optical response of plasmonic antennas," Optica **3**(3), 339–346 (2016).
68. R. Esteban, A. G. Borisov, P. Nordlander, and J. Aizpurua, "Bridging quantum and classical plasmonics with a quantum-corrected model," Nat. Commun. **3**(1), 825 (2012).
69. U. Kreibig and M. Vollmer, *Optical properties of metal clusters*, vol. 25 (Springer Science & Business Media, 2013).
70. J. Emsley, *Nature's Building Blocks: An A-Z Guide to the Elements* (Oxford University Press, 2003).
71. M. F. Laiza, F.-F. Romeu B., P.-d.-S. Marcelo A., V. Luis G., and G. L. Adabo, "Titanium surface topography after brushing with fluoride and fluoride-free toothpaste simulating 10 years of use," J. Dent. **40**(4), 265–275 (2012).